AGU PUBLICATIONS

JGR

Journal of Geophysical Research: Oceans

RESEARCH ARTICLE

10.1002/2014JC010007

Key Points:
- Diel cycles appear at each season with varying amplitudes and timings
- We show differences in the patterns of the diel variability of c_p and of b_{bp}
- c_p and b_{bp} diel cycles cannot be used interchangeably to infer production

Correspondence to:
M. Kheireddine,
kheireddine@obs-vlfr.fr

Citation:
Kheireddine, M., and D. Antoine (2014), Diel variability of the beam attenuation and backscattering coefficients in the northwestern Mediterranean Sea (BOUSSOLE site), *J. Geophys. Res. Oceans*, *119*, 5465–5482, doi:10.1002/2014JC010007.

Received 1 APR 2014
Accepted 26 JUL 2014
Accepted article online 30 JUL 2014
Published online 26 AUG 2014

Diel variability of the beam attenuation and backscattering coefficients in the northwestern Mediterranean Sea (BOUSSOLE site)

Malika Kheireddine[1,2] and David Antoine[1,2,3]

[1]Sorbonne Universités, Université Pierre et Marie Curie, Paris 06, UMR 7093, Laboratoire d'Océanographie de Villefranche, Observatoire Océanologique, Villefranche-sur-Mer, France, [2]Centre National de la Recherche (CNRS), UMR 7093, Laboratoire d'Océanographie de Villefranche, Observatoire Océanologique, Villefranche-sur-Mer, France, [3]Department of Imaging and Applied Physics, Remote Sensing and Satellite Research Group, Curtin University, Perth, Western Australia, Australia

Abstract The diel variability of the particulate beam attenuation coefficient, c_p, and of the particulate backscattering coefficient, b_{bp}, were investigated during five seasonal cycles at an oceanic site in the northwestern Mediterranean Sea, covering contrasting physical and trophic situations. We observed a diel cycle in c_p and b_{bp}, related to changes in phytoplankton properties (i.e., size and refractive index) induced by the accumulation of carbon within phytoplankton cells associated with photosynthetic processes, during the winter mixing of the water column, the development of the spring phytoplankton bloom, its decline, and during the summer oligotrophy. The relative amplitude of the c_p diel variability was much larger during the spring bloom (20–50%) than during other seasons (10–20%), whereas that of b_{bp} is steadily around 20% and does not show significant seasonal variability. The minimal c_p and b_{bp} occurred at sunrise and are synchronized, whereas maximum b_{bp} values are often reached 3–6 h before those for c_p (except during bloom conditions), which occur near sunset. These different amplitudes and timing are tentatively explained using Mie computations, which allow discerning the respective roles of changes in the particle size distribution and refractive index. The differences observed here in the diel cycles of c_p and b_{bp} show that they cannot be used interchangeably to determine the daily increase of the particle pool. This result has implications on the feasibility to determine net community production from the b_{bp} diel changes, when only b_{bp} is measured in situ or available from ocean color observations.

1. Introduction

Bio-optical relationships have long been established between inherent optical properties (IOPs) [in the sense of *Preisendorfer*, 1961] and biogeochemical parameters, such as the chlorophyll *a* concentration (Chl *a*) [*Bricaud et al*., 1995] and the particulate organic carbon (POC) [*Gordon and Morel*, 1983; *Gardner et al*., 1993; *Loisel and Morel*, 1998]. These relationships are used to derive information on biological and biogeochemical processes in the water column, from either in situ or satellite ocean color remote sensing observations [e.g., *Claustre et al*., 1999; *Stramski et al*., 1999]. They are established by pooling together data from different environments and are therefore global representations of the bio-optical variability. Most underlying processes, such as phytoplankton photosynthesis and particle growth and division, are associated to the daily light cycle. They accordingly exhibit a diel variability which is, however, not considered when building algorithms. This is partly responsible for the scatter in the relationships between IOPs and biogeochemical parameters.

Numerous studies were performed since the 1990s on the diel variability of IOPs in various oceanic regimes [*Siegel et al*., 1989; *Claustre et al*., 1999; *Gernez et al*., 2011]. They all used the particulate beam attenuation coefficient, c_p, as a proxy for the load of particles whose size is between about 0.5 and 20 μm [*Stramski and Kiefer*, 1991; *Pak et al*., 1988]. The particulate beam attenuation, c_p, is given by the sum of particulate scattering and absorption coefficients.

They suggested that the c_p diel variability is essentially associated with planktonic responses to the daily light cycle coupled to the dynamics of the upper mixed layer [*Siegel et al*., 1989; *Walsh et al*., 1995; *Stramski*

and Reynolds, 1993; *Durand and Olson*, 1998; *Durand et al*., 2002]. This diel variability is often observed in situ and can be replicated in the laboratory [*Claustre et al*., 2002] (although usually for monocultures only). Interpreting this variability is difficult, however, because it depends on numerous parameters, such as phytoplankton concentration, composition, and physiological status, but also concentrations of detritus and small heterotrophs. Full knowledge of the diel variability of each component is usually inaccessible, which means that the causes of the variations in optical properties remain poorly understood. They may include:

1. The balance between daytime production and nighttime degradation of biogenic particles (phytoplankton, bacteria, small heterotrophs), including phytoplankton excretion, cell division, and cell mortality (grazing activity and viral lyses) [*Cullen et al*., 1992; *Stramski and Reynolds*, 1993]. These biological responses depend on, e.g., temperature, nutrients availability, and light intensity [*Falkowski et al*., 1989; *Falkowski and Kolber*, 1995; *Stramski et al*., 2002; *Nelson and Prézelin*, 1990].
2. Changes in the particle size distribution.
3. Changes of refractive index driven by varying internal concentration of organic compounds (accumulation of intracellular carbon through photosynthesis).

Laboratory measurements have shown that (2) and (3) would be more important than changes in particle concentration in driving c_p diel variability [*Stramski and Reynolds*, 1993]. The impact of detrital particles on c_p diel variability is limited because they do not exhibit significant diel changes [*Durand and Olson*, 1996].

Recently, *Gernez et al*. [2011] have shown that c_p diel cycles display significant seasonal variability, which may result from seasonal changes in nutrient concentrations, phytoplankton abundance, size distribution, and composition. They also used the diel variations of c_p to estimate the corresponding change in the particulate organic carbon (POC), from which the net community production (NCP) can be derived [see also *Siegel et al*., 1989; *Claustre et al*., 2008].

Studying c_p diel variability is often motivated by the prospect of deriving NCP from satellite ocean color remote sensing observations, in particular those from a geostationary orbit [*Fishman et al*., 2012; *IOCCG*, 2012]. The particulate beam attenuation coefficient is not directly derivable from these observations, however. The IOP that is directly proportional to the ocean reflectance and can accordingly be derived from it is the particulate backscattering coefficient, b_{bp} [*Lee et al*., 2002; *Maritorena et al*., 2002; *Morel et al*., 2006], although deriving the beam attenuation coefficient from the reflectance has also been attempted [*Roesler and Boss*, 2003]. As for c_p, b_{bp} is, to first order, proportional to the particle load and, to second order, to the particle size distribution and to the refractive index, structure, and shape of particles.

Common belief would use existing relationships between both coefficients [e.g., *Dall'Olmo et al*., 2009; *Westberry et al*., 2010; *Antoine et al*., 2011] to derive the diel increase of c_p from that of b_{bp}. For this to be valid, a tight relationship between both coefficients should be observed, as well as parallel diel changes of the two coefficients (at least the same amplitude for the diel change). How existing relationships match the first requirement is unclear. The second requirement is, to our knowledge, totally undocumented. Therefore we analyzed here a 5 year (2006–2010) high-frequency (every 15 min) time series of c_p and b_{bp} at the BOUSSOLE (BOUée pour l'acquiSition d'une Série Optique à Long termE) site in the Mediterranean Sea [*Antoine et al*., 2006, 2008a, 2008b] with the main objective of comparing c_p and b_{bp} diel cycles under different environmental conditions (temperature, nutrients availability, and quantity and quality of light), in order to examine whether they could be interchangeably used to derive information on the daily increase of the particle pool. A second objective is to use theoretical Mie computations to evaluate whether particle size distribution or particle refractive index is more likely to drive the observed variability of c_p and b_{bp}.

2. Materials and Methods

2.1. Description of the BOUSSOLE Site and Related Field Operations

Essential information about the site characteristics, the measurement platforms and the instrumentation is provided in *Antoine et al*. [2006, 2008a,b]. Therefore, only information relevant to the present work is presented here. The BOUSSOLE site is located in deep waters (2440 m) of the Ligurian Sea, one of the subbasins of the Western Mediterranean Sea (Figure 1). Seasonal variations in vertical mixing (typically to 400 m in winter, and sometimes to the bottom) and stratification during summer appear to drive the seasonal

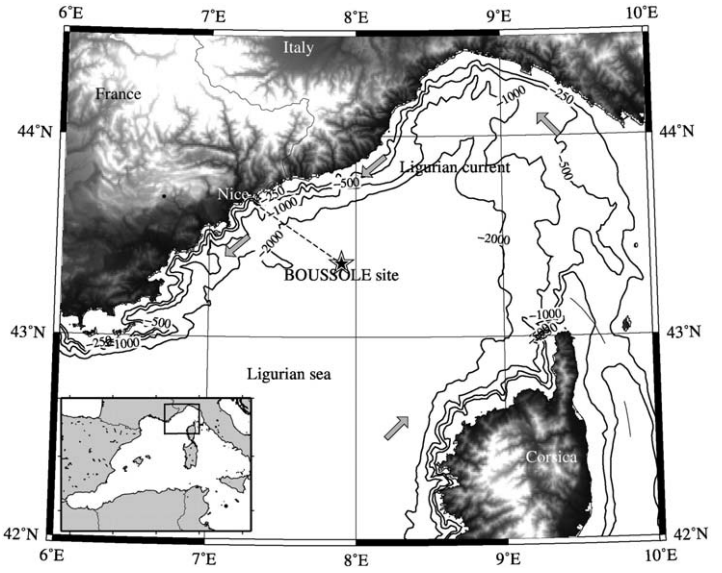

Figure 1. Map of the Northwestern Mediterranean Sea showing the location of the BOUSSOLE site in the Ligurian Sea (black star). Gray arrows show the main current flows.

changes in phytoplankton concentration and composition. Oligotrophic conditions prevail during summer when chlorophyll concentrations are below 0.1 mg m^{-3} (with minima ~0.05 mg m^{-3}). Higher concentrations, up to about 3–5 mg m^{-3}, occur during the spring bloom (February to March or April), and moderate concentrations (0.1–0.3 mg m^{-3}) the rest of the year. There is, accordingly, a large range of optical properties observed at this site [*Antoine et al*., 2006]. A buoy has been permanently deployed at the BOUSSOLE site since September 2003 and operates in a quasi-continuous mode, with data acquisition every 15 min night and day. IOPs are collected at two depths in the water column (nominally 4 and 9 m). Two sister buoys equipped with the same sets of instruments are used, with rotation performed about every 6 months. The site is visited monthly for buoy servicing, during which 0–400 m casts are performed for acquisition of hydrological data (conductivity, temperature, and density (CTD)), complementary IOPs and AOPs, and water sampling for subsequent phytoplankton pigment analyses and particulate absorption measurements. The buoy data used in this study are the particulate beam attenuation coefficient, c_p, the particulate backscattering coefficient, b_{bp}, the water temperature, salinity, and density. We use the phytoplankton pigment concentrations and mixed layer depth from the monthly cruise observations.

2.2. Backscattering Coefficient

The volume scattering function at 140°, $\beta(140)$, was initially measured at BOUSSOLE using HOBI Laboratories (Hydro-Optics, Biology, and Instrumentation Laboratories) Hydroscat-2 backscattering meters installed at the lower measurement depth of the buoy (~9 m) and equipped with filters at 442 and 550 nm. Starting in October 2007, HOBI Laboratories Hydroscat-4 backscattering meters were used, with bands at 442, 488, 550, and 620 nm. The instruments operate at 1 Hz, so that about 60 measurements are collected during each of the 1 min data collection sequence. The median of these 60 measurements is used to derive a representative value for $\beta(140)$. Dark current measurements are performed on site with a neoprene cap covering the instrument windows. Their average for a given 6 month deployment are subtracted from the raw $\beta(140)$ measurements. The $\beta(140)$ values are also corrected for attenuation along the measurement path (the $\sigma(\lambda)$ correction of *Maffione and Dana* [1997]) using the beam attenuation coefficient measured in parallel (see below) and the total absorption coefficient derived from inversion of the diffuse attenuation coefficient for downward irradiance (K_d) and the irradiance reflectance (R) [*Morel et al*., 2006, equations (12) and (13)]. The b_{bp} coefficient is derived from the corrected $\beta(140)$ as follows [*Maffione and Dana*, 1997; *Boss and Pegau*, 2001]:

$$b_{bp} = 2\pi\chi_p(\beta(140) - \beta_w(140)), \quad (1)$$

where $\chi_p = 1.13$ (D. R. Dana and R. A. Maffione, unpublished manuscript, 2014) and where $\beta_w(140)$, the contribution of pure seawater scattering at 140°, is computed following *Zhang et al*. [2009] and *Zhang and Hu* [2009] using the temperature and salinity measured at the same depth with a Seabird SBE-37SI CTD sensor. All results shown in this paper use the b_{bp} value at 550 nm.

2.3. Beam Attenuation Coefficient

The transmittance (*Tr*, %) at 660 nm is measured at BOUSSOLE at 4 and 9 m with 25 cm path length WET Laboratories (Western Environmental Technology Laboratories) C-Star transmissometers (acceptance angle

is 1.2°). Instruments are factory calibrated with deionized, ultrafiltered, UV-screened water. The corresponding particulate beam attenuation coefficient, c_p, is then calculated as:

$$c_p(660) = -\frac{1}{0.25}\ln\left(\frac{Tr}{100}\right).$$

This assumes that absorption by colored dissolved organic matter (CDOM) is negligible at 660 nm [*Bricaud et al*., 1981].

The instrument bodies are covered with copper tape. Source and detector windows are equipped with copper rings and are cleaned about every 2 weeks by divers using soft brushes. These measures have proven efficient in preventing biofouling in most cases. Possible remaining corrupted data are identified from the comparison of data collected before and after cleaning operations. They are eliminated and not used here.

The same instruments are deployed on the monthly casts, and their measurements are used to correct the buoy transmissometer data for possible calibration drifts.

2.4. Particulate Backscattering Ratio

The particulate backscattering ratio, $\tilde{b}_{bp}$, is defined as the ratio of the particle backscattering coefficient, b_{bp}, to the particle total scattering coefficient, b_p. Here a proxy to $\tilde{b}_{bp}$ is derived from b_{bp} and c_p as follows:

$$\widetilde{b_{bp}}(550) = \frac{b_{bp}(550)}{c_p(660)}, \quad (2)$$

which assumes that $c_p(660)$ is equal to the particle scattering coefficient at 660 nm, $b_p(660)$ (negligible absorption), and that b_p is spectrally flat between 550 and 660 ($b_p(550) = b_p(660\ \text{nm})$. The first assumption was validated by particulate absorption measurements using the quantitative filter pad technique, which shows an average $a_p(660)$ contribution to $c_p(660)$ of 2.5% only. The second assumption cannot be fully verified. The spectral dependence of the scattering coefficient is, however, typically within the [0–1] range when Chl decreases from about 2 to 0.02 mg m^{-3} [e.g., *Morel and Maritorena*, 2001], which means only a 10% uncertainty when the 550 nm to 660 nm spectral range is considered.

2.5. Phytoplankton Pigments

Pigment sampling is performed during the BOUSSOLE cruises between the surface and a depth of 200 m. Seawater samples are collected from Niskin bottles and filtered through 25 mm Whatman GF/F (0.7 μm) and then stored in liquid nitrogen until algae pigment contents are measured in the laboratory using High Performance Liquid Chromatography (HPLC), following *Ras et al*. [2008]. The total chlorophyll *a* concentration (TChl*a*) is computed as the sum of the concentrations of Chl *a*, chlorophyllide *a*, and divinyl Chl *a*. The data obtained from samples at 5 and 10 m are used here. The relative proportions of picophytoplankton (size < 2 μm), nanophytoplankton (2–20 μm), and microphytoplankton (20–200 μm) are determined from the concentration of phytoplankton pigments that have a taxonomic significance and can be associated with a size class, as described in *Uitz et al*. [2006]. The continuous record of average daily chlorophyll concentration (Chl a) used here is generated by combining the chlorophyll concentration determined from HPLC and the chlorophyll product of ocean colors sensors as described in *Antoine et al*. [2008a,b].

2.6. Physical Parameters

The water salinity (S, psu), water temperature (T, °C), and the buoy depth (*z*buoy, m) are measured with a Seabird SBE 37 SI CTD nominally installed at 9 m. The Sea Surface Temperature (SST, °C) and the wind speed (U, m s^{-1}) are measured hourly by a weather buoy moored two nautical miles away from BOUSSOLE, operated by the French weather forecast service, Meteo France. During the monthly cruises, vertical T and S profiles are performed using a Seabird SBE 911 plus CTD equipped with sensors for pressure (Digiquartz Paroscientific), temperature (SBE 3), and conductivity (SBE 4). After determination of the density, the mixed layer depth (*Zm*) is computed using a density gradient criterion of 0.125 kg m^{-3}.

2.7. Data Selection

Our goal is to characterize optical variations that result primarily from the ecosystem functioning. Unstable physical conditions may obscure the biologically driven diel cycle. Therefore, changes due to advection from, or mixing with, water masses of different optical properties have to be identified and eliminated from

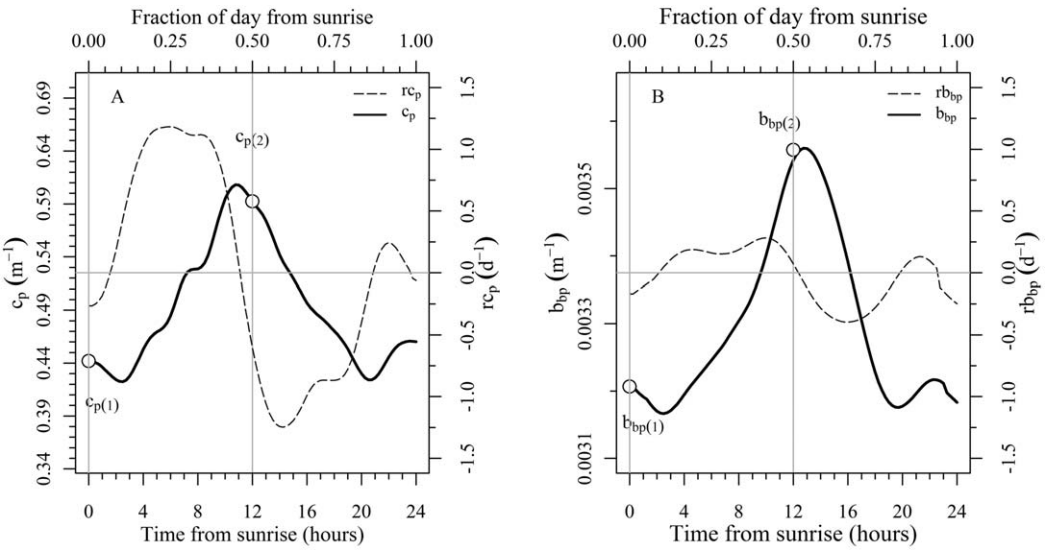

Figure 2. Example of diel cycles of (a) c_p and rc_p and (b) b_{bp} and rb_{bp}, as observed on 13 March 2006. The quantities $c_{p(1)}$, $c_{p(2)}$, $b_{bp(1)}$, and $b_{bp(2)}$ (equations (3) and (3′)) are indicated. Vertical lines indicate sunrise and sunset. The top axis represents fractions of the normalized day (sunset is 0.5).

the analysis. Essential information about how the data selection is performed using T, S, and SST is provided in *Gernez et al*. [2011]. The initial data set includes 1322 measurement days from which a subset of 737 days has been selected (≈43% of data measurements have been eliminated). Therefore, the assumption is made that the diel cycles in c_p and b_{bp} obtained here are not significantly affected by changes in the mixed layer depth and essentially result from biological activity [*Gernez et al*., 2011].

2.8. Characterization of the Diel Variability in c_p and b_{bp}

The amplitude of the diel variation in c_p (m^{-1}) and b_{bp} (m^{-1}) are, respectively,

$$\Delta c_p = c_{p(2)} - c_{p(1)}, \tag{3}$$

$$\Delta b_{bp} = b_{bp(2)} - b_{bp(1)}, \tag{3'}$$

where subscripts 1 and 2 indicate sunrise and sunset, respectively. The quantities derived through equations (3) and (3′) do not necessarily represent the maximum change, because the maximum of c_p, for instance, can be reached before sunset. An illustration is provided in Figure 2.

The relative variation from sunrise (in %) is defined by:

$$\tilde{\Delta} c_p(k) = 100\ [c_{p(k)}/c_{p(1)} - 1], \tag{4}$$

$$\tilde{\Delta} b_{bp}(k) = 100\ [b_{bp(k)}/b_{bp(1)} - 1], \tag{4'}$$

where k is a fraction of a day. Fraction of the day are used, rather than hours, in order to allow comparison between days of varying photoperiod, whereby k is 0 at sunrise, 0.25 at noon, 0.5 at sunset, and 1 at the next sunrise.

The instantaneous specific rates of variation in optical properties which are related to particles (in day^{-1}) is computed as:

$$rc_p(t) = (1/c_p)\ \delta c_p/\delta t, \tag{5}$$

$$rb_{bp}(t) = (1/b_{bp})\ \delta b_{bp}/\delta t, \tag{6}$$

where δc_p or δb_{bp} is the variation within the time between two consecutive measurements ($\delta t = 15$ min).

3. Results

The 5 year time series of daily averages of c_p, b_{bp} (550 nm), Chl a, and Z_m is displayed in Figure 3. The seasonal variations of *Zm* show two distinct regimes, with a period of mixing from about December to February

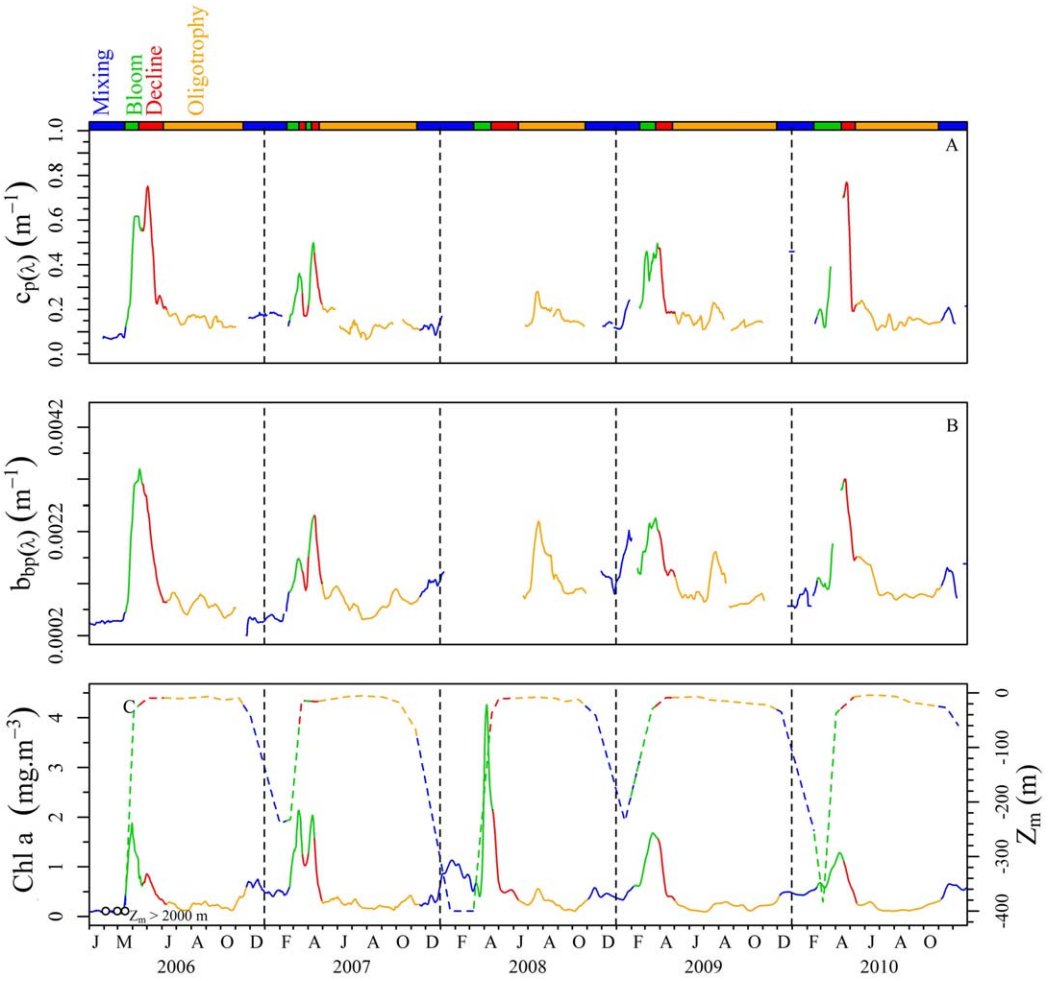

Figure 3. Time series of daily mean values of c_p, b_{bp}, Chl a, and Zm. The color bars on top of each figure indicate the segmentation in the four seasons defined in Table 1.

($Z_m \sim 400$ m), a period of rapid shallowing of the mixed layer at the beginning of Spring (around March–April), and a period of stratification the rest of the year, i.e., during summer and of the first half of fall. The year 2006 was marked by an exceptional deep mixing in January–March ($Zm > 2000$ m). The seasonal variations in mixing and stratification appear to drive the seasonal changes phytoplankton composition and concentration. High values occur during spring then decrease about 2 months later, after which concentrations remain low throughout the rest of the year. Generally, c_p and b_{bp} vary in parallel to TChl from February to June.

Seasonal changes in the phytoplankton size structure are observed at the BOUSSOLE site with larger cells (microphytoplankton) generally dominating during the end of winter and the beginning of the spring bloom (February–March), nanophytoplankton dominating from April to June, picophytoplankton dominating from August to December, and mixed communities during January–February (Figure 4). The dominance by picophytoplankton is not exceptional and has also been observed at the end of summer in the 1990s and in 2000 and 2001 at or near the BOUSSOLE site [*Gernez et al*., 2011]. Note that microphytoplankton dominate the biomass only during the spring bloom in 2006 while nanophytoplankton dominate during the spring bloom from 2007 to 2010. The switch between nano and microphytoplankton dominated blooms is also a feature of this area: microphytoplankton dominated during the bloom of years 2000 and 2005 [*Organelli et al*., 2013] while the bloom was dominated by nanophytoplankton during the other years.

In order to study the c_p and b_{bp} diel variability over time intervals where environmental conditions are reasonably stable, the data set has been segmented into four distinct situations: winter mixing, spring phytoplankton bloom, decline of the bloom, and summer and fall oligotrophy. This grouping is based on *Zm* and TChl characteristics following *Gernez et al*. [2011]. Selection criteria and mean characteristics of these

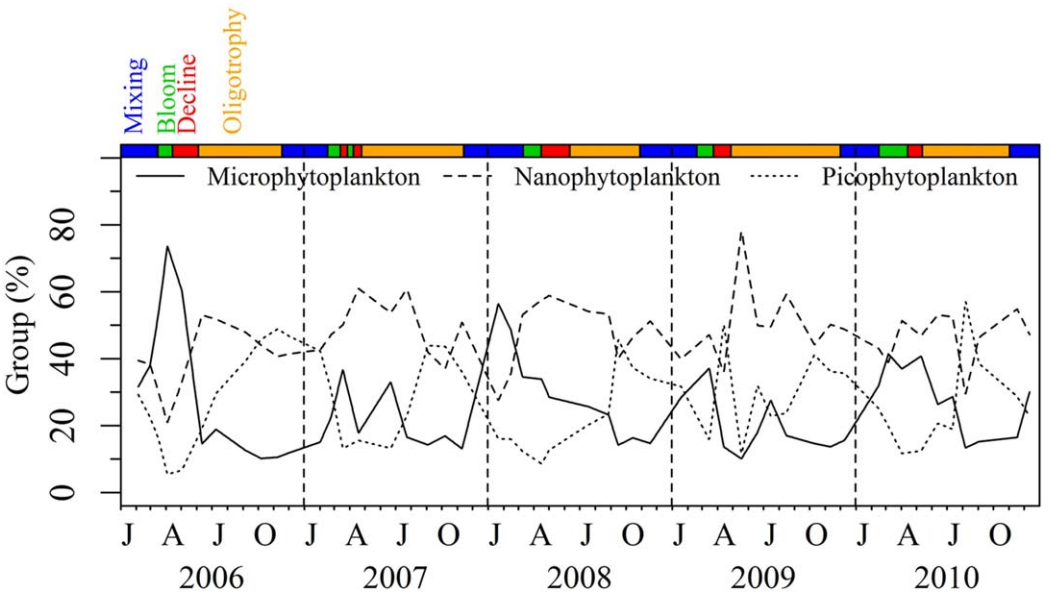

Figure 4. Temporal evolution of the pico, nano, and microphytoplankton from pigments signature obtained by HPLC. The color bars on top of each figure indicate the segmentation in the four seasons defined in Table 1.

seasons are indicated in Table 1. The term "season" is used for the sake of simplicity, although the defined periods do not necessarily match the winter-spring-summer-fall calendar. The diel variability is now examined for each season, first as a few typical examples, and then as average cycles for each season.

Typical examples of diel cycles of c_p and b_{bp} are displayed in Figures 5a and 5b for the four seasons. The same data are shown in Figures 5c–5f in terms of relative daily changes ($\tilde{\Delta}c_p$ and $\tilde{\Delta}b_{bp}$). A diel cycle appears to be a recurrent feature in the c_p and b_{bp} data at the BOUSSOLE site. Differences in the shape and amplitude of the diel changes are observed at different periods of the year, which indicates that the physical and trophic states have an effect on this variability of c_p and b_{bp}. Whatever the season, the minimal c_p and b_{bp} occur around sunrise and are synchronized whereas maximum b_{bp} are often reached 3–6 h before those for c_p, which occur just before sunset. The weakest daily changes ($\tilde{\Delta}c_p$ and $\tilde{\Delta}b_{bp}$) are observed during the mixing period (Figure 5c), with values around or below 15%. The daily changes are slightly larger during the summer oligotrophy, with values between 15 and 20%. The largest changes are logically observed during the two phases of the bloom (i.e., increase and decline), with values up to 350% for $\tilde{\Delta}c_p$ and 180% for $\tilde{\Delta}b_{bp}$.

The daily averaged percent variation from sunrise, $\tilde{\Delta}c_p$, is shown for each season (Figures 6a–6d) and each year separately (Figures 7a–7d). A diel cycle clearly appears whatever the season and year. The timing is nearly the same at all seasons: $\tilde{\Delta}c_p$ starts increasing at dawn and reaches a maximum at or just before sunset (i.e., between 0.4 and 0.5 days), in agreement with previous observations performed in various oligotrophic and mesotrophic ecosystems [*Siegel et al*., 1989; *Claustre et al*., 1999, 2008; *Gernez et al*., 2011; *Loisel et al*., 2011]. The average amplitude is of 10–25% during the mixing, bloom decline, and oligotrophic periods, and of 25%–40% during the bloom. The standard deviation is generally of the same order of magnitude than the mean and is maximal during the bloom (Tables 2 and 3).

A diel cycle also appears for $\tilde{\Delta}b_{bp}$ whatever the season (Figures 6e–6h) and year (Figures 7e–7h). The maximum of $\tilde{\Delta}b_{bp}$ is, generally, reached earlier than the one for $\tilde{\Delta}c_p$, except during the bloom where maxima for

Table 1. Selection Criteria and Characteristics of the Four Seasons Differentiated From the BOUSSOLE Time Series Within Which Average Parameters of the c_p and b_{bp} Diel Cycles Are Determined

Season	Physical Conditions	Chl a (mg m^{-3})	Average Size Particles
Mixing	Mixing, Zm > 80 m		Largest (8–50 μm)
Bloom	Stratification	>0.6 (↑)	Largest and large (4–50 μm)
Decline	Stratified	>0.45 (↓)	Large and small (2–20 μm)
Oligotrophy	Stratified	<0.45 (stable)	Smallest (0.2–2 μm)

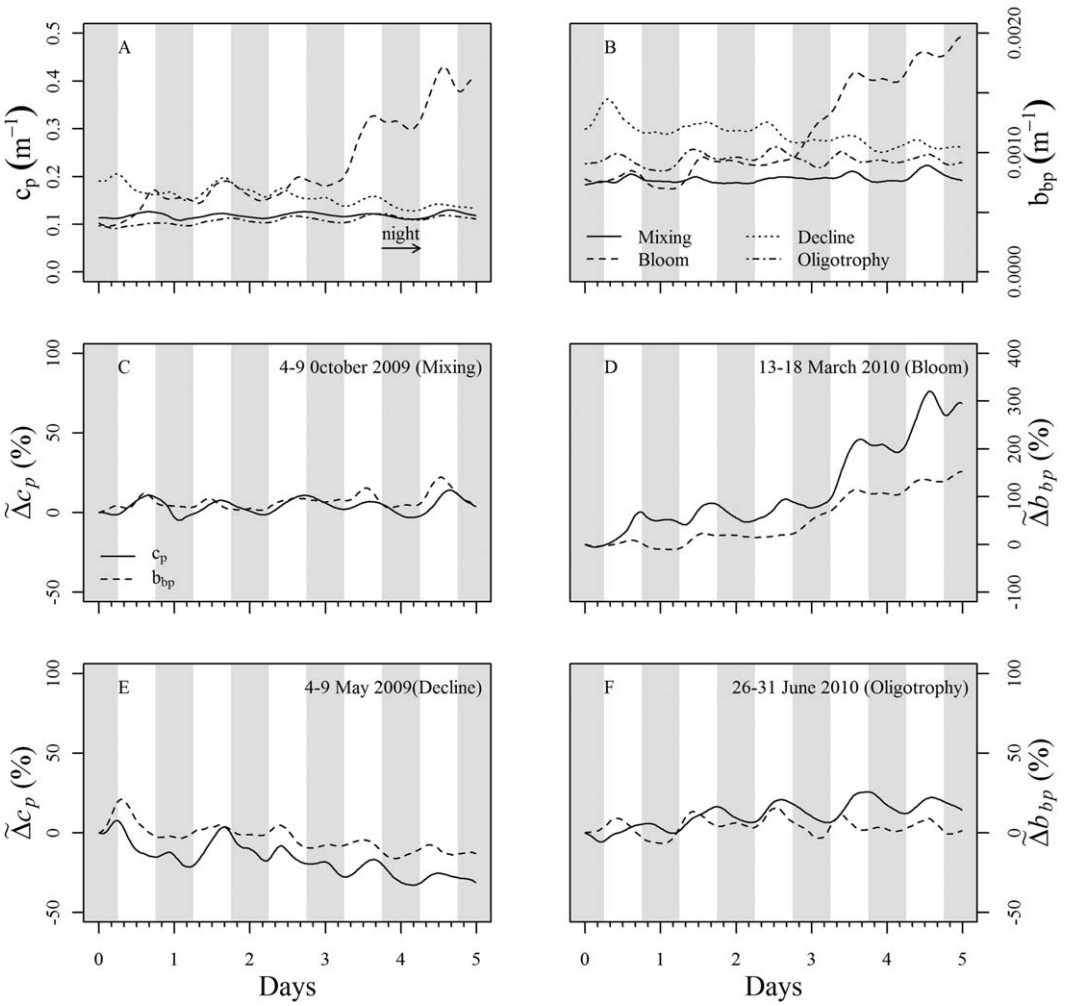

Figure 5. Examples of 5 day time series of (a) c_p and (b) b_{bp} chosen within each of the four seasons (as indicated in Figure 5b). The corresponding daily percent variation ($\tilde{\Delta}c_p$ and $\tilde{\Delta}b_{bp}$) are displayed in Figures 5c–5f. Gray areas indicate nighttime.

the two coefficients nearly coincide. In order to quantify these time lags, we performed a cross correlation between c_p and b_{bp} diel cycles for each season, by shifting the c_p diel cycles toward morning or evening by up to 6 h. We estimated the correlation between the shifted cycles, rc_pb_{bp}, for each of the shifts (Figure 8). The maximum correlation is achieved for a time lag of -3.75 ± 1.75 h during the mixing period (Figure 8a), -3 ± 1 h during the bloom decline (Figure 8c), and -3.5 ± 1.5 h during oligotrophy (Figure 8d). During bloom conditions, the maximum correlation is obtained when cycles are not shifted (Figure 8b). The amplitude of $\tilde{\Delta}b_{bp}$ is between 5 and 38% according to the season. The spring bloom does not show significantly larger $\tilde{\Delta}b_{bp}$ than for other seasons. Interannual variations are small for $\tilde{\Delta}c_p$, except for the bloom and bloom decline conditions (Figures 6 and 7a–7d). They seem larger for $\tilde{\Delta}b_{bp}$, which on the contrary does not show large seasonal changes. In contrast, the diel cycles of c_p and b_{bp} are the most regular during oligotrophy.

The rates of variation for c_p and b_{bp}, rc_p and rb_{bp}, emphasize differences in their diel cycles. The rates are displayed in Figures 6 and 7i–7l for c_p and Figures 6 and 7m–7p for b_{bp}. The seasonal variation in the amplitude of the c_p diel cycles is confirmed, with rc_p within $\sim\pm 0.6$ d^{-1} during the mixing, bloom decline, and the oligotrophic periods and up to ~ 1.4 d^{-1} during the bloom. The maximum rc_p is slightly before noon. Then rc_p decreases and becomes negative before sunset. Variations observed during the night are usually small during the mixing, bloom decline (except for 2007), and oligotrophic periods, with constant negative values until midnight and a slow recovery in the second half of the night.

The rate of variation for backscattering, rb_{bp}, varies between 0.3 and 2 d^{-1} (Figures 6 and 7m–7p) and shows an increase during the first half of the morning, a maximum around noon (between 0.15–0.45 days),

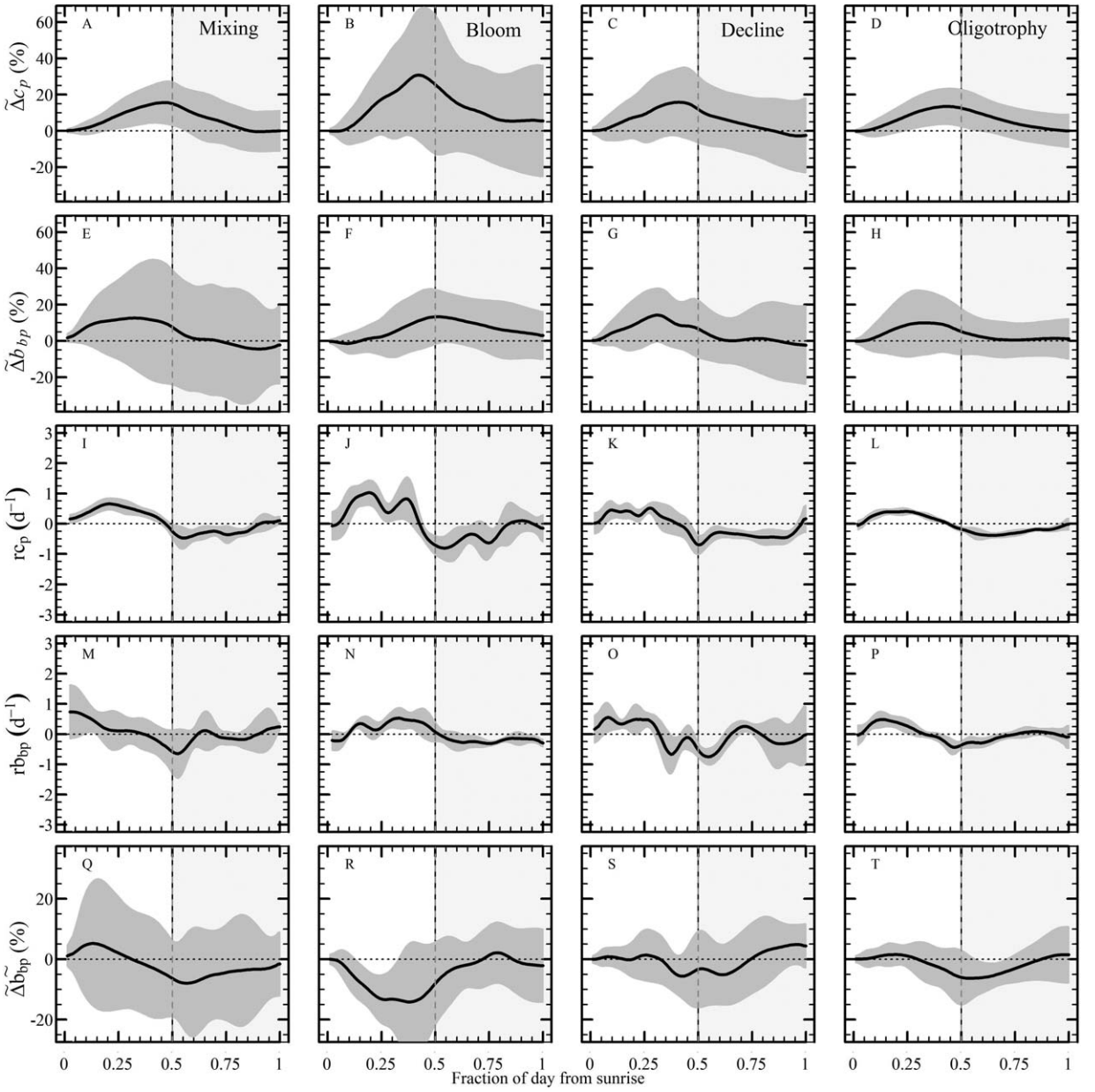

Figure 6. Average $\tilde{\Delta}c_p$, $\tilde{\Delta}b_{bp}$, rc_p, rb_{bp}, and $\tilde{\Delta}\widetilde{b_{bp}}$ (from top to bottom) (±standard deviation, SD: gray area) during the four seasons defined in Table 1 (from left to right: mixing, bloom, decline, and oligotrophy, years from 2006 to 2010). The *x* axis represents fractions of the day (i.e., sunset is 0.5 and midday is 0.25 whatever the season).

and decreasing values during the afternoon. The rb_{bp} becomes negative 3–6 h before sunset, which is consistent with the maximum of b_{bp} being reached before sunset. Except during the phytoplankton bloom period, rb_{bp} decreases and becomes negative before sunset as for rc_p. Nighttime variations are observed whatever the season.

To further highlight differences in daily cycles of c_p and b_{bp}, their ratio, i.e., the particulate backscattering ratio, $\tilde{\Delta}\tilde{b}_{bp}$, is displayed in Figures 6 and 7q–7t. This ratio is sensitive to the refractive index of particles and their size distribution and is therefore an indicator of the bulk nature of the particulate matter [*Twardowski et al.*, 2001; *Boss et al.*, 2004]. A diel cycle clearly appears whatever the season and year. $\tilde{\Delta}\widetilde{b_{bp}}$ starts decreasing at dawn and starts increasing, generally, at sunset. The timing is nearly the same at all seasons. The differences observed in maxima of c_p and b_{bp}, described previously, engender small differences in timing of maxima of $\tilde{\Delta}\widetilde{b_{bp}}$. Minima of $\tilde{\Delta}\widetilde{b_{bp}}$ are observed around sunset (±3–6 h). The amplitude is around 10% during the mixing (except for 2006), decline, and oligotrophy periods, and around 20% during the phytoplankton bloom.

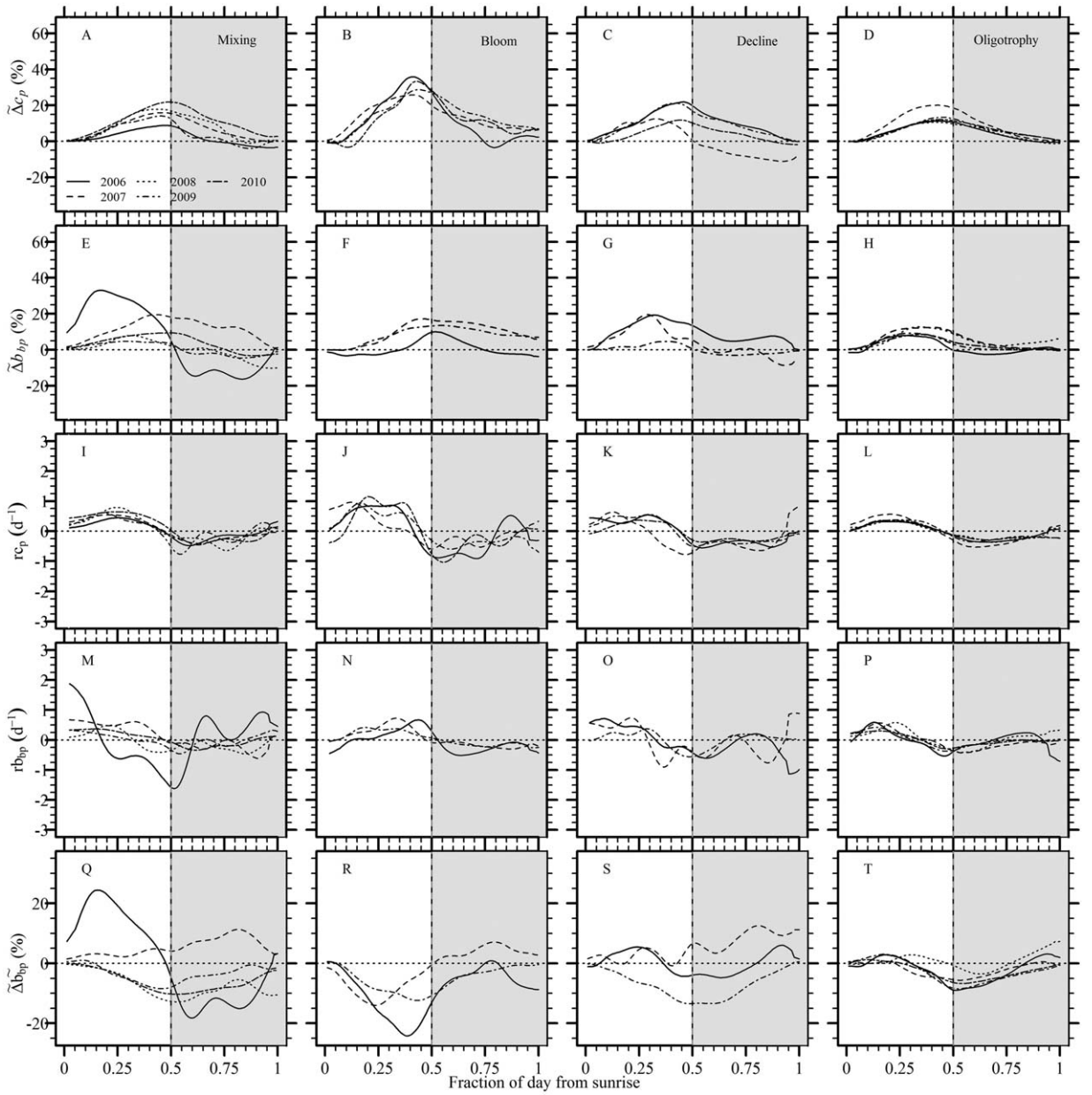

Figure 7. Average $\tilde{\Delta}c_p$, $\tilde{\Delta}b_{bp}$, rc_p, rb_{bp}, and $\tilde{\Delta}\widetilde{b_{bp}}$ (from top to bottom) during the four seasons as in Figure 6. Average cycles for each of the 5 years from 2006 to 2010 are superimposed in each figure (see line coding in Figure 7a). The *x* axis represents fractions of the day (i.e., sunset is 0.5 and midday is 0.25 whatever the season).

4. Discussion

4.1. Plausible Origins of the c_p and b_{bp} Diel Variability

Our data set does not include the observations that would allow a full understanding of the causes for the diel cycles of c_p and b_{bp} and for their differences in amplitude and timing. This would require a detailed knowledge of the composition and optical properties of suspended particulate matter, i.e., particles concentration, sizes, and refractive index, at the same frequency than the IOPs. This is not the situation when using the BOUSSOLE data set and is seldom available from field measurements. We can nevertheless examine whether our observations are consistent with current knowledge about which processes occur in the upper ocean that lead either to a decrease or an increase in the particle load, or to changes in particle characteristics (size and refractive index). The increase of c_p during the lighted portion of the day is usually explained by the accumulation of intracellular carbon concentration associated with photosynthetic processes, which

Table 2. Mean and Standard Deviation of the Daily Averaged $\tilde{\Delta}c_p$ Shown in Figure 6

Mean $\tilde{\Delta}c_p \pm$ SD (%)	2006	2007	2008	2009	2010	Mean by Season	Number of Days Analyzed
Mixing	18 ± 16	19 ± 10	18 ± 9	14 ± 8	22 ± 15	16 ± 11	65
Bloom	38 ± 52	27 ± 24	NA	29 ± 26	34 ± 36	31 ± 38	59
Collapse	24 ± 16	15 ± 12	NA	21 ± 14	12 ± 11	16 ± 20	54
Decline	15 ± 11	20 ± 16	11 ± 7	14 ± 7	12 ± 8	14 ± 9	397
Mean by year	19 ± 12	18 ± 8	14 ± 7	20 ± 11	19.5 ± 12		

implies changes in phytoplankton properties, particularly an increase in refractive index and size [*Siegel et al*., 1989; *Walsh et al*., 1995; *Stramski and Reynolds*, 1993; *Durand and Olson*, 1998; *Claustre et al*., 2002; *Durand et al*., 2002]. At any time of day and night, losses of particulate matter occur in relation to respiration and phytoplankton excretion, cell division, and cell mortality (grazing activity and viral lyses) [*Stramski and Reynolds*, 1993; *Cullen et al*., 1992].

The daily amplitude of the c_p cycles (Figures 6 and 7a–7d) is larger during the bloom, i.e., when phytoplankton cells are neither light-limited nor nutrient-limited, as compared to winter mixing, bloom decline, and oligotrophy, during which phytoplankton cells are either light-limited or nutrient-limited or both. *Reynolds et al*. [1997] have shown that that the amplitude of diel variability in phytoplankton absorption and attenuation decreases under nitrogen-limited growth. This is consistent with laboratory studies that have shown that light-limited or nutrient-limited phytoplankton have a low production rate of phytoplanktonic carbon via photosynthesis [*Falkowski et al*., 1989; *Falkowski and Kolber*, 1995; *Stramski et al*., 2002; *Nelson and Prézelin*, 1990]. There is an adjustment of the physiological activity according to the environmental conditions (quantity and quality of nutrients and light field), which tends to decrease the contribution of phytoplankton to the c_p daily changes. Bacteria, zooplankton (grazers), and detritus also contribute to the c_p variability. Because they likely do not vary at the diel scale [*Durand and Olson*, 1996], an increase in their proportion relative to phytoplankton will lower the daily percent amplitude of c_p. The shape of the c_p diel cycle is different during the bloom of 2006 as compared to the other years. This might be related to differences in phytoplanktonic composition: in 2006, the bloom was dominated by microphytoplankton, whereas nanophytoplankton dominated from 2007 to 2010 (Figure 4).In contrast to c_p diel cycles, b_{bp} diel cycles are not marked by a significant seasonal variability. This would confirm that phytoplankton makes a smaller contribution to b_{bp} than to c_p, so their seasonal changes poorly reflect in seasonal changes of $\tilde{\Delta}b_{bp}$. Backscattering is more sensitive to the presence of submicrometer particles such as detrital particles or heterotrophic bacteria (according to Mie theory: *Morel and Ahn* [1991] and *Stramski and Kiefer* [1991]), which all have little reason to show recurrent diel variability. Therefore, their steady presence damps the relative b_{bp} diel variability.

The differences observed in the timing of c_p and b_{bp} diel maxima might be related to an increase in the small sized phytoplankton cells induced by cell divisions at different times of the day. *Vaulot and Marie* [1999] have shown a synchronization of picoplankton population with a temporal gap of a few hours between *Prochlorococcus, Synechococcus*, and picoeukaryotes. Others have shown that Chlorophyceae and Euglenophyceae divide generally during the night whereas diatoms show peaks of division during daytime and at night [*Sournia*, 1974; *Smayda*, 1975; *Williamson*, 1980].

The decrease of the backscattering ratio during the day (Figures 6 and 7q–7t) suggests either a decrease of the refractive index or a decreasing proportion of small particles relatively to large particles or both. We assumed that the refractive index of the cell population is a real number (i.e., absorption is neglected at

Table 3. Mean and Standard Deviation of the Daily Averaged $\tilde{\Delta}b_{bp}$ Shown in Figure 6

Mean $\tilde{\Delta}b_{bp} \pm$ SD (%)	2006	2007	2008	2009	2010	Mean by Season	Number of Days analyzed
Mixing	35 ± 57	21 ± 35	9 ± 21	5 ± 5	9.5 ± 18	12 ± 35	69
Bloom	10 ± 17	18 ± 18	NA	13 ± 18	NA	13 ± 16	39
Collapse	20 ± 31	21 ± 37	NA	5 ± 8	NA	14 ± 17	32
Decline	8 ± 28	12 ± 34	13 ± 18	9.5 ± 9	9 ± 8	10 ± 16	322
Mean by year	12 ± 18	16 ± 8	9 ± 11	7 ± 7	9 ± 5		

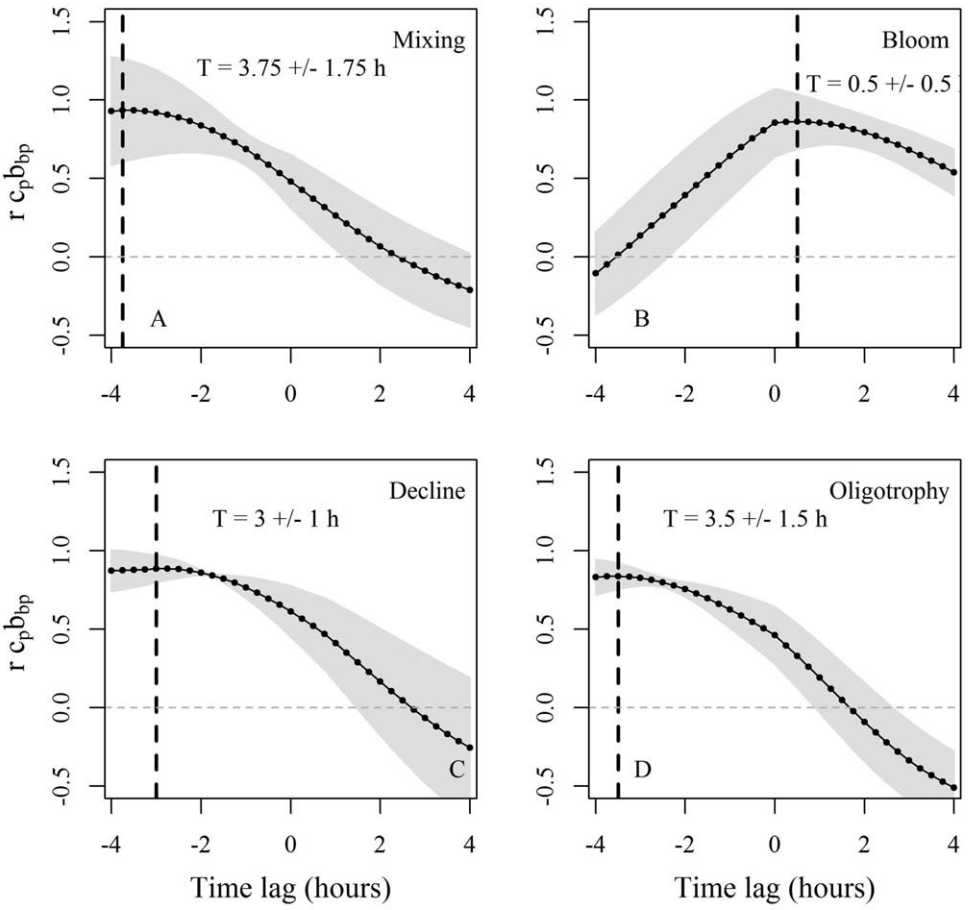

Figure 8. Cross correlation between c_p and b_{bp} diel cycles during the four seasons: (a) mixing, (b) bloom, (c) bloom decline, and (d) oligotrophy. The black dashed line represents the time lag at which maxima of c_p and b_{bp} diel cycles are best correlated. The gray dashed line indicates that $rc_pb_{bp} = 0$. The gray area represents the standard deviation (SD) of rc_pb_{bp}. The average time lag (T) (±SD) at which maxima are best correlated is indicated on each figure.

550 nm). The first cause is unlikely, because the increase in c_p and b_{bp} rather indicates an increase in intracellular carbon concentration, which should lead to an increase in refractive index. The negative $\tilde{\Delta}\widetilde{b_{bp}}$ rather results from changes in particles shape and size distribution, which suggests that the PSD is the main factor controlling the $\tilde{b}_{bp}$ diel cycles. This is consistent with *Loisel et al.* [2007], who showed that the slope of the PSD was the main factor controlling the $\tilde{b}_{bp}$ variability in case 1 waters whereas the refractive index had more importance in case 2 waters.

4.2. Interpreting Observed Daily Changes Through Mie Computations

In order to further evaluate plausible causes of the c_p and b_{bp} diel changes, theoretical computations have been performed using Mie theory, as driven by assumptions about how the various optically significant compartments evolve over a day. The goal is not to reproduce specific observations of any single day in our data set. We rather aim at exploring whether realistic assumptions on the daily changes in the particle size distribution (PSD) and refractive index (n) can lead to realistic average amplitudes and timing of the c_p and b_{bp} daily changes. The results of such computations are discussed by keeping in mind the known limitations of Mie theory, which is, strictly speaking, only valid for spherical and homogeneous particles. Therefore, it is used here as an imperfect yet useful tool for interpretation of our observations.

The strategy has been to establish as a starting point a population of particles representative of clear oligotrophic waters. Patterns of diel variability of n, PSD, and abundance of phytoplankton cells are subsequently applied, from typical results of previous studies [*Stramski and Reynolds*, 1993; *André et al.*, 1999; *Durand et al.*, 2002; *Durand and Olson*, 1998; *Claustre et al.*, 2002; *Stramski et al.*, 1995; *Vaulot et al.*, 1995; *Liu et al.*, 1997].

Table 4. Concentration, Particle Size Range, Refractive Index, and Growth and Mortality Rates of Each Group of Microorganisms Used in Mie Computations, Which Were All Performed for a Wavelength of 660 nm

Component	Concentration[a] (m^{-3})	Size Range[a] (μm)	n[b]
Viruses	7.0×10^{16}	0.01–0.3	1.08
Bacteria	3.0×10^{15}	0.1–1.2	1.075
Detritus	5.0×10^{14}	0.02–4	1.08
Picophytoplankton	1.0×10^{14}	0.2–2	1.05
Ultrananoplankton	5.0×10^{12}	2–8	1.05
Nanophytoplankton	1.5×10^{11}	8–20	1.05
Microphytoplankton	1.0×10^{10}	20–100	1.05

[a] *Stramski and Kiefer* [1991].
[b] *Stramski and Reynolds* [1993], *Stramski et al.* [1995], *Aas* [1996], and *Green et al.* [2003].

The input parameters for each category of particle are the numerical concentration, the size distributions (minimum, mean, and maximum diameters, and standard deviation), and the refractive index. Computations were performed for a single wavelength (660 nm), which is that of field c_p measurements and where particle and CDOM absorption are negligible and consequently not modeled here. We included viruses, detritus, heterotrophic bacteria, picophytoplankton (0.2–2 μm), ultrananophytoplankton (2–8 μm), larger nanophytoplankton (8–20 μm), and microphytoplankton (>20 μm). Realistic concentrations of these components were chosen so that their cumulative size distribution roughly obeys an inverse fourth power law in cell diameter, from 0.03 to 100 μm. The real part of the refractive index varied between 1.05 and 1.08 according to the category of particles [*Aas*, 1996; *Green et al.*, 2003] (Table 4). We assume that the imaginary part of the refractive index is neglected (i.e., absorption is negligible at 660 nm).

The c_p and b_{bp} coefficients were modeled as the sum of constant background components, c_p0 and $b_{bp}0$ ($t = 0$), and time-varying components, c_p1 and $b_{bp}1$. It was chosen to make c_p1 and $b_{bp}1$ depending only on the four phytoplankton populations (pico, ultrananno, nano, and microphytoplankton), whereas all other components (virus, bacteria, and detritus) are kept constant over time. It is assumed that the cell abundance varied only because of the processes of cell division and mortality (grazing and cell mortality) [*Stramski and Reynolds*, 1993; *Stramski et al.*, 1995; *André et al.*, 1999; *Durand and Olson*, 1998; *Claustre et al.*, 2002; *Durand et al.*, 2002].

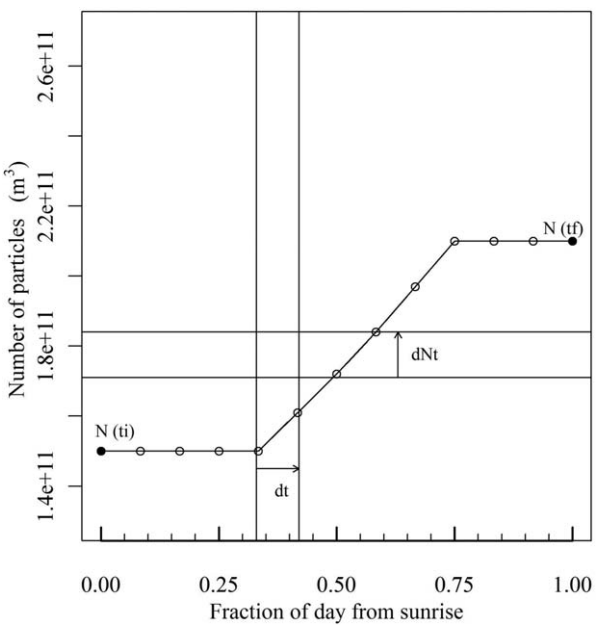

Figure 9. An example of how cell abundance (here for nanophytoplankton) is made varying during a diel cycle (equation 7). Black dots are the initial and final cell numbers (N(ti) and N(tf). The horizontal axis represents fractions of a normalized day (sunset is 0.5).

A simple model was used to reproduce the abundance of phytoplankton cells during a diel cycle, where the cell number, N(t), varies over a time step dt by dN(t), according to:

$$dN(t) = [\mu_d - g]\, N(t)\, dt, \quad (7)$$

where μd and g are the instantaneous division and mortality rates during the period of division, respectively (see Figure 9). We choose, arbitrarily, to make μ_d and g not to vary temporally during this period. The daily division and mortality rates corresponded to an average of results for different phytoplankton groups (pico, nano, or microphytoplankton) [*André et al.*, 1999; *Carpenter and Chang*, 1988; *Cullen et al.*, 1992; *Liu et al.*, 1995, 1997; *McDuff and*

Table 5. Growth and Mortality Rates of Phytoplankton Groups for Different Environmental Conditions: Oligotrophy, Bloom, and Decline Period Used in Mie Computations [*Calbet and Landry*, 2004, and References Therein; *Chen and Liu*, 2010; *Chen et al*., 2013, and References Therein]

Environmental Conditions	Oligotrophy	Bloom	Decline
Picophytoplankton	$\mu_d = 0.8$	$\mu_d = 0.8$	$\mu_d = 0.8$
	$g = 0.77$	$g = 0.65$	$g = 0.89$
Ultrananophytoplankton	$\mu_d = 0.55$	$\mu_d = 1$	$\mu_d = 0.55$
	$g = 0.49$	$g = 0.49$	$g = 0.63$
Nanophytoplankton	$\mu_d = 0.50$	$\mu_d = 0.9$	$\mu_d = 0.50$
	$g = 0.43$	$g = 0.43$	$g = 0.57$
Microphytoplankton	$\mu_d = 0.35$	$\mu_d = 0.42$	$\mu_d = 0.35$
	$g = 0.29$	$g = 0.29$	$g = 0.42$

Chisholm, 1982; *Peters*, 1994; *Calbet and Landry*, 2004, and references therein] (see Table 5). A typical example of imposed daily changes in n, mean size, and the particle abundance is shown in Figure 10.

As a first step, modeled $\tilde{\Delta}c_p$ and $\tilde{\Delta}b_{bp}$ are presented in Figure 11 for three distinct simplified cases: (1) when a diel variation is applied only to the phytoplankton PSD (Figure 11a), (2) only to the refractive index of phytoplankton, n (Figure 11b), and (3), to both PSD and n (Figure 11c). The two first cases are unrealistic and only used to quantify the influence of the two parameters separately. They confirm that the main driving factor for c_p diel changes is the PSD, whereas changes in the refractive index have more influence on b_{bp} diel changes. With these simplistic cases, neither the amplitude nor the timing of the diel cycles is consistent with our observations, however. Getting realistic diel changes for the two coefficients, both in terms of amplitude and timing, requires daily changes in both PSD and n (Figure 11c). These results are obviously dependent on the choices we made on input parameters (e.g., Figure 10).

Similarly, $\tilde{\Delta}c_p$ and $\tilde{\Delta}b_{bp}$ have been modeled for different periods of cell division: (1) the cell division period of all phytoplankton groups occurs just a few hours before sunset and (2) the cell division period of picophytoplankton cells occurs at a different time, more precisely in mid-afternoon, in contrast to other phytoplankton groups. Results (not shown) reproduce well the differences observed in the timing of c_p and b_{bp} diel maxima as observed (Figure 8).

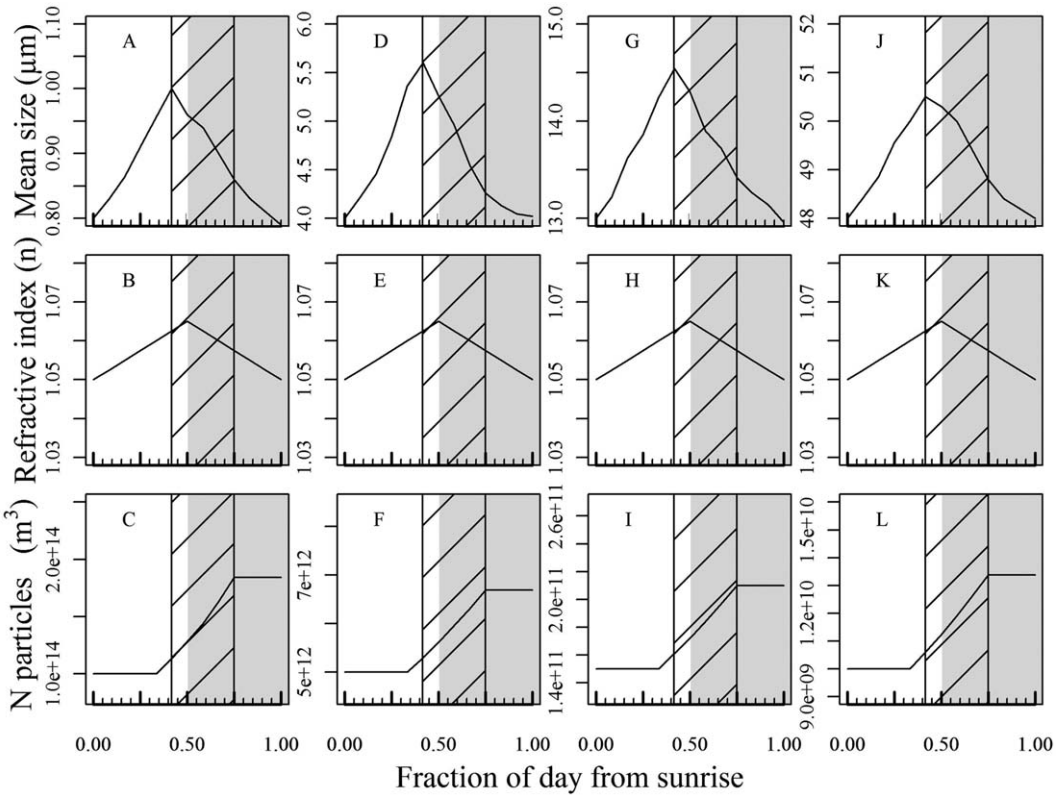

Figure 10. An example of the diel variations of cell properties and abundance imposed as input to Mie computations (see text). Figures 10a–10c are for picophytoplankton, (d–f) for ultrananophytoplankton, (g–i) for nanophytoplankton, and (j–l) for microphytoplankton during situations of oligotrophy. The hashed area is the cell division period and the shaded area is nighttime.

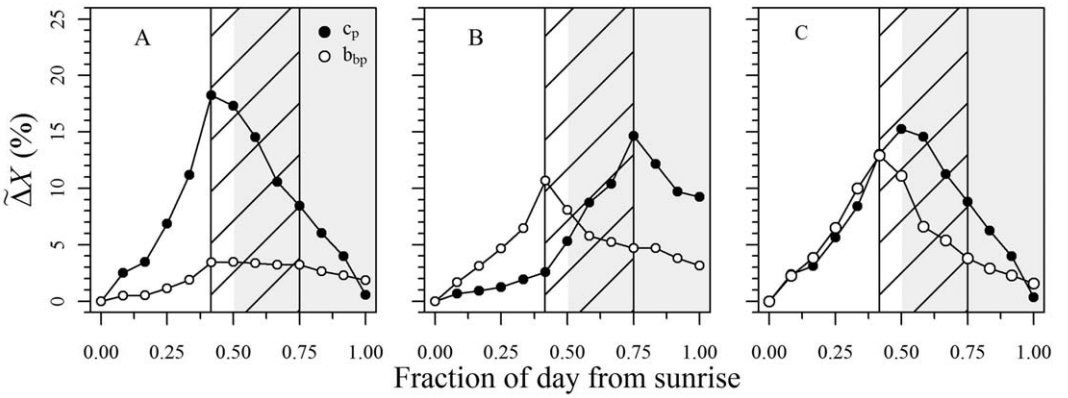

Figure 11. Average $\tilde{\Delta}cp$ (black dots) and $\tilde{\Delta}b_{bp}$ (open circles) for a variation of either (a) size only or (b) refractive index only or (c) both. The hashed area is the cell division period and the shaded area is nighttime.

The model has been subsequently used to represent three of the seasons identified here, i.e., the bloom development and decline, and the summer oligotrophy (Table 5). The resulting $\tilde{\Delta}c_p$ and $\tilde{\Delta}b_{bp}$ are presented in Figures 12a–12c. They reproduce well the c_p and b_{bp} diel cycles and their seasonal differences as observed in our data set (Figures 5–7).

We caution against over interpretation of these results because of inevitable uncertainties associated with the assumptions of particle sphericity and homogeneity required in the Mie theory. These assumptions can influence the prediction of scattering, especially backscattering, compared with real arbitrarily shaped, nonuniform particles [e.g., *Clavano et al*., 2007; *Zaneveld and Kitchen*, 1995]. Despite these limitations, Mie theory offers a useful tool for the analysis of relative variations in scattering and backscattering coefficients. The assumptions inherent to the MIE theory do not introduce major errors in the estimation of the relative roles of the abundance, PSD and n in the backscattering properties. This is because changes in abundance, PSD and n, rather than variations in particulate shape or heterogeneity, are the first-order determinant of the backscattering coefficient. Furthermore, studies have shown that optical properties, including the backscattering coefficient, are primarily dependent on the particles size and weakly dependent on their shape, and therefore are very close to those properties for spherical particles [*Asano and Sato*, 1980; *Ulloa et al*., 1994].

The role of PDS changes on the c_p and b_{bp} diel variability could be further validated by using a method such that published by *Briggs et al*. [2013]. This method allows deriving particle size from high-frequency fluctuation of beam attenuation and backscattering coefficients and providing additional information given that c_p and b_{bp} are sensitive to different sized particles.

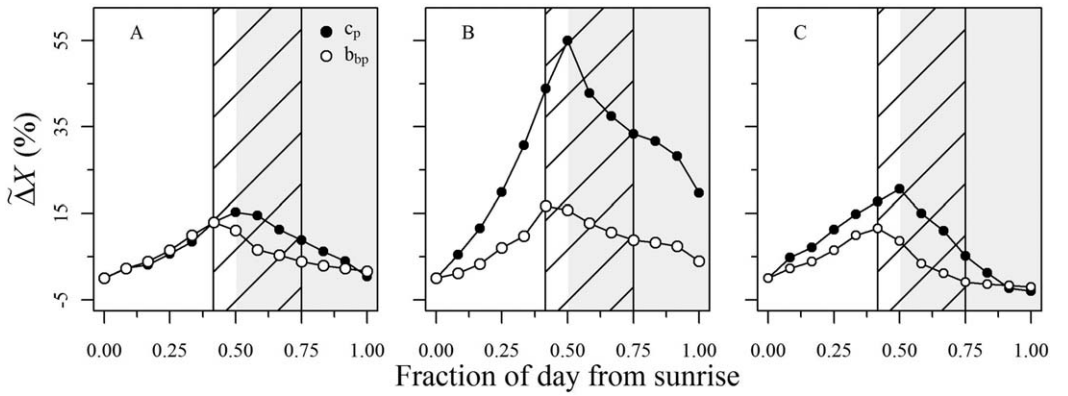

Figure 12. Average $\tilde{\Delta}cp$ (black dots) and $\tilde{\Delta}bbp$ (open circles) during situations of (a) oligotrophy, (b) bloom development, and (c) bloom decline. The hashed area is the cell division period and the shaded area is nighttime.

4.3. Using b_{bp} Diel Changes to Infer c_p Diel Changes?

Comparable c_p and b_{bp} diel changes would allow using them interchangeably to derive information on the daily increase of the particle pool, which is related to the net community production of the ecosystem [*Siegel et al*., 1989; *Claustre et al*., 2008; *Gernez et al*., 2011]. This possibility arises from the reasonably good correlation observed between c_p and b_{bp} [e.g., *Dall'Olmo et al*., 2009; *Westberry et al*., 2010; *Antoine et al*., 2011]. This suggests that when c_p is not available (e.g., from inversion of ocean color remote sensing observations), deriving it from b_{bp} might be indirectly feasible. The global relationships between c_p and b_{bp} made from an assemblage of punctual observations taken at various times of the day ignore the fact that c_p and b_{bp} do not vary in parallel over a day (Figures 5–7), with the maximum in b_{bp} occurring earlier than the one in c_p, for instance. The amplitude of the b_{bp} diel changes is nearly insensitive to the trophic state, whereas that of c_p is markedly different during bloom conditions. These observations show that using either field observations or satellite-derived values of b_{bp} to indirectly infer c_p through their relationship might be feasible with moderate accuracy. Deriving $\tilde{\Delta}c_p$ from $\tilde{\Delta}b_{bp}$, however, is apparently not an avenue to determining NCP from either field measurements or satellite-derived b_{bp}. Global b_{bp} versus c_p relationships [*Dall'Olmo et al*., 2009; *Westberry et al*., 2010; *Antoine et al*., 2011] are primarily driven by the particle load, whereas the composition and size distribution of particles and, as shown in this study, the different diel cycles are responsible for the scatter in the relationship between c_p and b_{bp}. The BOUSSOLE time series includes majority of oligotrophic conditions. We cannot, therefore, completely rule out the possibility to infer biogeochemical quantities from diel changes in b_{bp} on the basis of this sole data set, in spite of its significant and unprecedented length. Major upwelling areas, as well as basin-scale phytoplankton blooms, e.g., the northern Atlantic spring bloom, are areas where the diel changes in b_{bp} might be significant enough to allow determining NCP from the backscattering signal. Specific studies of the diel variability of IOPs are therefore needed in such areas. Whenever feasible, they should include measurements of the quantities that are necessary for a better understanding of the origins of the b_{bp} variability, such as the particle size distribution and refractive index, or the composition of the living and detrital particle pools.

Acknowledgments

We thank D.G. Bowers and the two anonymous reviewers for their comments on the initial manuscript. Annick Bricaud, Hervé Claustre, and Vincenzo Vellucci are warmly thanked for their suggestions on early versions on this paper. The authors are grateful to the BOUSSOLE technical staff for their work in performing laboratory analyses, buoy deployments, and monthly cruises, and to the captains and crews of R/V Téthys-II, Antea, and Europe. In particular, our thanks go to Emilie Diamond and Melek Golbol for the monthly cruises, Joséphine Ras and Mustapha Ouhssain for the HPLC pigment analyses, Vincenzo Vellucci and Bernard Gentili for the optical data calibration and processing. This study is a contribution to the Bio-optics and Carbon Experiment (BIOCAREX) project, which is funded by the Agence Nationale de la Recherche (ANR, Paris), and to the BOUSSOLE project. Multiple organizations support BOUSSOLE and provide technical and logistic support: the European Space Agency (ESA), the Centre National d'Etudes Spatiales (CNES), the Centre National de la Recherche Scientifique (CNRS), the National Aeronautics and Space Administration of the USA (NASA), the Institut National des Sciences de l'Univers (INSU), the Université Pierre et Marie Curie (UPMC), and the Observatoire Océanologique de Villefranche sur Mer (OOV). M.K. benefited from a grant provided by CNES and the region Provence Alpes Côte d'Azur (PACA). The data presented in this study are available on the BOUSSOLE website (http://www.obs-vlfr.fr/Boussole).

References

Aas, E. (1996), Refractive index of phytoplankton derived from its metabolite composition, *J. Plankton Res.*, *18*, 2223–2249, doi:10.1093/plankt/18.12.2223.

Andre, J. M., C. Navarette, J. Blanchot, and M. H. Radenac (1999), Picophytoplankton dynamics in the equatorial Pacific: Growth and grazing rates from cytometric counts, *J. Geophys. Res.*, *104*, 3369–3380, doi:10.1029/1998JC900005.

Antoine, D., et al. (2006), BOUSSOLE: A joint CNRS-INSU, ESA, CNES and NASA Ocean Color Calibration And Validation Activity, *NASA Technical memorandum N°2006 – 214147*, 61 pp.

Antoine, D., F. d'Ortenzio, S. B. Hooker, G. Becu, B. Gentili, D. Tailliez, and A. J. Scott (2008a), Assessment of uncertainty in the ocean reflectance determined by three satellite ocean color sensors (MERIS, SeaWiFS and MODIS-A) at an offshore site in the Mediterranean Sea (BOUSSOLE project), *J. Geophys. Res.*, *113*, C07013, doi:10.1029/2007JC004472.

Antoine, D., P. Guevel, J. F. Deste, G. Becu, F. Louis, A. J. Scott, and P. Bardey (2008b), The "BOUSSOLE" buoy—A new transparent-to-swell taut mooring dedicated to marine optics: Design, tests, and performance at sea, *J. Atmos. Oceanic Technol.*, *25*, 968–989, doi:10.1175/2007jtecho563.1.

Antoine, D., D. A. Siegel, T. Kostadinov, S. Maritorena, N. B. Nelson, B. Gentili, V. Vellucci, and N. Guillocheau (2011), Variability in optical particle backscattering in contrasting bio-optical oceanic regimes, *Limnol. Oceanogr. Methods*, *56*, 955–973, doi:10.4319/lo.2011.56.3.0955.

Asano, S., and M. Sato (1980), Light scattering by randomly oriented spheroidal particles, *Appl. Opt.*, *19*, 962–974, doi:10.1364/AO.19.000962.

Boss, E., and W. S. Pegau (2001), Relationship of light scattering at an angle in the backward direction to the backscattering coefficient, *Appl. Opt.*, *40*, 5503–5507, doi:10.1364/ao.40.005503.

Boss, E., W. S. Pegau, M. Lee, M. S. Twardowski, E. Shybanov, G. Korotaev, and F. Baratange (2004), Particulate backscattering ratio at LEO 15 and its use to study particles composition and distribution, *J. Geophys. Res.*, 109:C01014, doi:10.1029/2002JC001514.

Bricaud, A., A. Morel, and L. Prieur (1981), Absorption by dissolved organic matter of the sea (yellow substance) in the UV and visible domains, *Limnol. Oceanogr.*, *26*, 43–53.

Bricaud, A., M. Babin, A. Morel, and H. Claustre (1995), Variability in the chlorophyll specific absorption coefficients of natural phytoplankton: Analysis and parametrization, *J. Geophys. Res.*, *100*, 13,321–13,332, doi:10.1029/95JC00463.

Briggs, N. T., W. H. Slade, E. Boss, and M. J. Perry (2013), Method for estimating mean particle size from high-frequency fluctuations in beam attenuation or scattering measurements, *Appl. Opt.*, *52*, 6710–6725.

Calbet, A., and M. R. Landry (2004), Phytoplankton growth, microzooplankton grazing, and carbon cycling in marine systems, *Limnol. Oceanogr. Methods*, *49*, 51–57.

Carpenter, E. J., and J. Chang (1988), Species-specific phytoplankton growth rates via diel DNA synthesis cycles. 1. Concept of the method, *Mar. Ecol. Prog. Ser.*, *43*, 105–111, doi:10.3354/meps043105.

Chen, B., L. Zheng, B. Huang, S. Song, and H. Liu (2013), Seasonal and spatial comparisons of phytoplankton growth and mortality rates due to microzooplankton grazing in the northern South China Sea, *Biogeosciences*, *10*, 2775–2785, doi:10.5194/bg-10-2775-2013.

Chen, B. Z., and H. B. Liu (2010), Relationships between phytoplankton growth and cell size in surface oceans: Interactive effects of temperature, nutrients, and grazing, *Limnol. Oceanogr. Methods*, *55*, 965–972, doi:10.4319/lo.2010.55.3.0965.

Claustre, H., A. Morel, M. Babin, C. Cailliau, D. Marie, J. C. Marty, D. Tailliez, and D. Vaulot (1999), Variability in particle attenuation and chlorophyll fluorescence in the tropical Pacific: Scales, patterns, and biogeochemical implications, *J. Geophys. Res.*, *104*, 3401–3422, doi:10.1029/98JC01334.

Claustre, H., A. Bricaud, M. Babin, F. Bruyant, L. Guillou, F. Le Gall, D. Marie, and F. Partensky (2002), Diel variations in *Prochlorococcus* optical properties, *Limnol. Oceanogr.*, *47*, 1637–1647.

Claustre, H., Y. Huot, I. Obernosterer, B. Gentili, D. Tailliez, and M. Lewis (2008), Gross community production and metabolic balance in the South Pacific Gyre, using a non intrusive bio-optical method, *Biogeosciences*, *5*, 463–474.

Clavano, W. R., E. Boss, and L. Karp-Boss (2007), Inherent optical properties of non-spherical marine-like particles—From theory to observation, *Oceanogr. Mar. Biol. Annu. Rev.*, *45*, 1–38.

Cullen, J. J., M. R. Lewis, C. O. Davis, and R. T. Barber (1992), Photosynthetic characteristics and estimated growth rates indicating grazing is the proximate control of primary production in the Equatorial Pacific, *J. Geophys. Res.*, *97*, 639–654, doi:10.1029/91JC01320.

Dall'Olmo, G., T. K. Westberry, M. J. Behrenfeld, E. Boss, and W. H. Slade (2009), Significant contribution of large particles to optical backscattering in the open ocean, *Biogeosciences*, *6*, 947–967.

Durand, M. D., and R. J. Olson (1996), Contributions of phytoplankton light scattering and cell concentration changes to diel variations in beam attenuation in the equatorial Pacific from flow cytometric measurements of pico-, ultra- and nanoplankton, *Deep Sea Res., Part II*, *43*, 891–906, doi:10.1016/0967-0645(96)00020-3.

Durand, M. D., and R. J. Olson (1998), Diel patterns in optical properties of the chlorophyte Nannochloris sp.: Relating individual-cell to bulk measurements, *Limnol. Oceanogr.*, *43*, 1107–1118.

Durand, M. D., R. E. Green, H. M. Sosik, and R. J. Olson (2002), Diel variations in optical properties of *Micromonas pusilla* (Prasinophyceae), *J. Phycol.*, *38*, 1132–1142, doi:10.1046/j.1529-8817.2002.02008.x.

Falkowski, P. G., and Z. Kolber (1995), Variations in chlorophyll fluorescence yields in phytoplankton in the world's oceans, *Aust. J. Plant Physiol.*, *22*, 341–355.

Falkowski, P. G., A. Sukenik, and R. Herzig (1989), Nitrogen limitation in *Isochrysis galbana* (Haptophyceae). 2. Relative abundance of chloroplast proteins, *J. Phycol.*, *25*, 471–478, doi:10.1111/j.1529-8817.1989.tb00252.x.

Fishman, J., et al. (2012), The United States next generation of atmospheric composition and coastal ecosystem measurements NASA's Geostationary Coastal and Air Pollution Events (GEO-CAPE) Mission, *Bull. Am. Meteorol. Soc.*, *93*, 1547, doi:10.1175/bams-d-11-00201.1.

Gardner, W. D., I. D. Walsh, and M. J. Richardson (1993), Biophysical forcing of particle production and distribution during a spring bloom in the North Atlantic, *Deep Sea Res., Part II*, *40*, 171–195, doi:10.1016/096760645(93)90012-C.

Gernez, P., D. Antoine, and Y. Huot (2011), Diel cycles of the particulate beam attenuation coefficient under varying trophic conditions in the northwestern Mediterranean Sea: Observations and modeling, *Limnol. Oceanogr. Methods*, *56*, 17–36, doi:10.4319/lo.2011.56.1.0017.

Gordon, H. R., and A. Morel (1983), *Remote Assessment of Ocean Color for Interpretation of Satellite Visible Imagery: A Review*, Springer, N. Y.

Green, R. E., H. M. Sosik, and R. J. Olson (2003), Contributions of phytoplankton and other particles to inherent optical properties in New England continental shelf waters, *Limnol. Oceanogr. Methods*, *48*, 2377–2391.

IOCCG (2012), Ocean-colour observations from a geostationary orbit, in *Reports of the International Ocean-Colour Coordinating Group, Rep. 12*, 5–28, edited by D. Antoine, Dartmouth, Canada.

Lee, Z. P., K. L. Carder, and R. A. Arnone (2002), Deriving inherent optical properties from water color: A multiband quasi-analytical algorithm for optically deep waters, *Appl. Opt.*, *41*, 5755–5772, doi:10.1364/ao.41.005755.

Liu, H. B., L. Campbell, and M. R. Landry (1995), Growth and mortality rates of *Prochlorococcus* and *Synechococcus* measured with a selective inhibitor technique, *Mar. Ecol. Prog. Ser.*, *116*, 277–287, doi:10.3354/meps116277.

Liu, H. B., H. A. Nolla, and L. Campbell (1997), *Prochlorococcus* growth rate and contribution to primary production in the equatorial and subtropical North Pacific Ocean, *Aquat. Microb. Ecol.*, *12*, 39–47, doi:10.3354/ame012039.

Loisel, H., and A. Morel (1998), Light scattering and chlorophyll concentration in case 1 waters: A reexamination, *Limnol. Oceanogr.*, *43*, 847–858.

Loisel, H., X. Meriaux, J.-F. Berthon, and A. Poteau (2007), Investigation of the optical backscattering to scattering ratio of marine particles in relation to their biogeochemical composition in the eastern English Channel and southern North Sea, *Limnol. Oceanogr. Methods*, *52*, 739–752.

Loisel, H., et al. (2011), Characterization of the bio-optical anomaly and diurnal variability of particulate matter, as seen from scattering and backscattering coefficients, in ultra-oligotrophic eddies of the Mediterranean Sea, *Biogeosciences*, *8*, 3295–3317, doi:10.5194/bg-8-3295-2011.

Maffione, R. A., and D. R. Dana (1997), Instruments and methods for measuring the backward-scattering coefficient of ocean waters, *Appl. Opt.*, *36*, 6057–6067, doi:10.1364/ao.36.006057.

Maritorena, S., D. A. Siegel, and A. R. Peterson (2002), Optimization of a semianalytical ocean color model for global-scale applications, *Appl. Opt.*, *41*, 2705–2714, doi:10.1364/ao.41.002705.

McDuff, R. E., and S. W. Chisholm (1982), The calculation of in situ growth rates of phytoplankton populations from fraction of cells undergoing mitosis: A clarification, *Limnol. Oceanogr.*, *27*, 783–788.

Morel, A., and Y.-H. Ahn (1991), Optics of heterotrophic nanoflagellates and ciliates: A tentative assessment of their scattering role in oceanic waters compared to those of bacterial and algal cells, *J. Mar. Res.*, *49*, 177–202.

Morel, A., and S. Maritorena (2001), Bio-optical properties of oceanic waters: A reappraisal, *J. Geophys. Res.*, *106*, 7163–7180, doi:10.1029/2000JC000319.

Morel, A., B. Gentili, M. Chami, and J. Ras (2006), Bio-optical properties of high chlorophyll Case 1 waters and of yellow-substance-dominated Case 2 waters, Deep Sea Res., Part I, *53*, 1439–1459, doi:10.1016/j.dsr.2006.07.007.

Nelson, N. B., and B. B. Prezelin (1990), Chromatic light effects and physiological modeling of absorption properties of *Heteroscapsa pygmaea* (=Glenodymium sp.), *Mar. Ecol. Prog. Ser.*, *63*, 37–46, doi:10.3354/meps063037.

Organelli, E., A. Bricaud, D. Antoine, and J. Uitz (2013), Multivariate approach for the retrieval of phytoplankton size structure from measured light absorption spectra in the Mediterranean Sea (BOUSSOLE site), *Appl. Opt.*, *52*, 2257–2273.

Pak, H., D. A. Kiefer, and J. C. Kitchen (1988), Meridional variations in the concentration of chlorophyll and microparticles in the North Pacific Ocean, *Deep Sea Res., Part I*, *35*, 1151–1171, doi:10.1016/0198-0149(88)90007-6.

Peters, F. (1994), Prediction of planktonic protistan grazing rates, *Limnol. Oceanogr.*, *39*, 195–206.

Preisendorfer, R. W. (1961), Application of radiative transfer theory to light measurements in the sea, *Monogr. Int. Union Geod. Geophys. Paris*, *10*, 11–30.

Ras, J., H. Claustre, and J. Uitz (2008), Spatial variability of phytoplankton pigment distributions in the Subtropical South Pacific Ocean: Comparison between in situ and predicted data, *Biogeosciences*, *5*, 353–369.

Reynolds, R. A., D. Stramski, and D. A. Kiefer (1997), The effect of nitrogen limitation on the absorption and scattering properties of the marine diatom *Thalassiosira pseudonana*, *Limnol. Oceanogr.*, *42*, 881–892.

Roesler, C. S., and E. Boss (2003), Spectral beam attenuation coefficient retrieved from ocean color inversion, *Geophys. Res. Lett.*, *30*(9), 1468, doi:10.1029/2002GL016185.

Siegel, D. A., T. D. Dickey, L. Washburn, M. K. Hamilton, and B. G. Mitchell (1989), Optical determination of particulate abundance and production variations in the oligotrophic ocean, *Deep Sea Res., Part A*, *36*, 211–222, doi:10.1016/0198-0149(89)90134-9.

Smayda, T. J. (1975), Phased cell division in natural populations of marine diatom *Ditylum brightwelli* and potential significance of diel phytoplankton behavior in sea, *Deep Sea Res. Oceanogr. Abstr.*, *22*, 151–165, doi:10.1016/0011–7471(75)90055-8.

Sournia, A. (1974), Circadian periodicities in natural populations of marine phytoplankton, *Adv. Mar. Biol.*, *12*, 325–389.

Stramski, D., and D. A. Kiefer (1991), Light scattering by microorganisms in the open ocean, *Prog. Oceanogr.*, *28*, 343–383, doi:10.1016/0079–6611(91)90032-h.

Stramski, D., and R. A. Reynolds (1993), Diel variations in the optical properties of a marine diatom, *Limnol. Oceanogr.*, *38*, 1347–1364.

Stramski, D., A. Shalapyonok, and R. A. Reynolds (1995), Optical characterisation of the oceanic unicellular cyanobacterium *Synechococcus* grown under a day-night cycle in natural irradiance, *J. Geophys. Res.*, *100*, 13,295–13,307, doi:10.1029/95jc00452.

Stramski, D., R. A. Reynolds, M. Kahru, and B. G. Mitchell (1999), Estimation of particulate organic carbon in the ocean from satellite remote sensing, *Science*, *285*, 239–242, doi:10.1126/science.285.5425.239.

Stramski, D., A. Sciandra, and H. Claustre (2002), Effects of temperature, nitrogen, and light limitation on the optical properties of the marine diatom *Thalassiosira pseudonana*, *Limnol. Oceanogr.*, *47*, 392–403.

Twardowski, M. S., E. Boss, J. B. Macdonald, W. S. Pegau, A. H. Barnard, and J. R. V. Zaneveld (2001), A model for estimating bulk refractive index from the optical backscattering ratio and the implications for understanding particle composition in case I and case II waters, *J. Geophys. Res.*, *106*, 14,129–14,142, doi:10.1029/2000JC000404.

Uitz, J., H. Claustre, A. Morel, and S. Hooker (2006), Vertical distribution of phytoplankton communities in open ocean: an assessment based on surface chlorophyll, *J. Geophys. Res.*, *111*, C08005, doi:10.1029/2005JC003207.

Ulloa, O., S. Sathyendranath, and T. P. Latt (1994), Effect of the particle-size distribution on the backscattering ratio in seawater, *Appl. Opt.*, *33*, 7070–7077, doi:10.1364/AO.33.007070.

Vaulot, D., and D. Marie (1999), Diel variability of photosynthetic picoplankton in the equatorial Pacific, *J. Geophys. Res.*, *104*, 3297–3310, doi:10.1029/98JC01333.

Vaulot, D., D. Marie, R. J. Olson, and S. W. Chisholm (1995), Growth of *Prochlorococcus*, a photosynthetic prokaryote, in the equatorial pacific ocean, *Science*, *268*, 1480–1482, doi:10.1126/science.268.5216.1480.

Walsh, I. D., S. P. Chung, M. J. Richardson, and W. D. Gardner (1995), The diel cycle in the integrated particle load in the equatorial pacific: A comparison with primary production, *Deep Sea Res., Part II*, *42*, 465–477, doi:10.1016/0967-0645(95)00030-t.

Westberry, T. K., G. Dall'Olmo, E. Boss, M. J. Behrenfeld, and T. Moutin (2010), Coherence of particulate beam attenuation and backscattering coefficients in diverse open ocean environments, *Opt. Express*, *18*, 15,419–15,425.

Williamson, C. E. (1980), Phased cell division in natural and laboratory populations of marine planktonic diatoms, *J. Exp. Mar. Biol. Ecol.*, *43*, 271–279, doi:10.1016/0022-0981(80)90052-0.

Zaneveld, J. R. V., and J. C. Kitchen (1995), The variation in the inherent optical properties of phytoplankton near an absorption peak as determined by various models of cell structure, *J. Geophys. Res.*, *100*, 13,309–13,320, doi:10.1029/95JC00451.

Zhang, X. D., and L. B. Hu (2009), Estimating scattering of pure water from density fluctuation of the refractive index, *Opt. Express*, *17*, 1671–1678.

Zhang, X. D., L. B. Hu, and M. X. He (2009), Scattering by pure seawater: Effect of salinity, *Opt. Express*, *17*, 5698–5710.